Impact of the C1′ Configuration of Abasic Sites on DNA Duplex Structure[†,‡]

Carlos de los Santos,* Mahmoud El-khateeb, Pankaj Rege, Kegui Tian, and Francis Johnson

Department of Pharmacological Sciences, School of Medicine, State University of New York, Stony Brook, New York 11794-8651

Received July 27, 2004; Revised Manuscript Received September 21, 2004

ABSTRACT: Naturally occurring abasic sites in DNA exist as an equilibrium mixture of the aldehyde, the hydrated aldehyde, and the hemiacetal forms (dominant). The influence of the configuration of the C1′ hydroxyl group of the hemiacetal form on duplex structure and abasic site repair has been examined using novel carbocyclic analogues. Both the α- and β-forms of this novel abasic site were introduced into oligomeric DNA using the standard DMT-phosphoramidite approach in an automated solid-phase synthesizer. Solution structures of the d(CGTACXCATGC)·d(GCATGAGTACG) duplex (where X is the α- or β-anomer of the carbocyclic abasic site analogue) were determined by NMR spectroscopy and restrained molecular dynamics simulations. The structures were only minimally perturbed by the presence of either anomer of the abasic site. All residues adopted an *anti* conformation, and Watson−Crick alignments were observed on all base pairs of the duplexes. At the lesion site, the abasic residues and their partner adenines showed increased dynamic behavior but adopted intrahelical positions in the final refined structures. Incision of duplexes having the α- or β-anomer of the carbacyclic abasic site by human AP endonuclease showed that the enzyme recognizes both configurations of the lesion and nicks the DNA backbone with similar efficiency. Our results challenge the suggestion that Ape1 is stereoselective and imply a plasticity at the active site of the enzyme for accommodating either anomer of the lesion.

Hydrolysis of the *N*-glycosylic bond in DNA results in the loss of nucleobases and formation of apurinic/apyrimidinic sites (abasic sites or AP[1] sites). It has been estimated that at 37 °C and pH 7.4 spontaneous depurination produces between 9000 and 14 000 AP sites per cell per day (*1*, *2*). *N*7-Alkylation of purine bases and some exocyclic adducts accelerates the depurination rate, thereby increasing the repair burden of abasic sites in genomic DNA (*3*, *4*). In addition, some frequent endogenous lesions such as deoxyuracil residues, originating from cytosine deamination, or etheno bases, generated by lipid peroxidation products, are processed by base excision repair, which produces AP sites as repair intermediates (*5*). Abasic sites are noncoding lesions that may cause mutations and cytotoxicity during DNA replication (*3*). DNA and RNA polymerases stall at an AP site in the template strand, but the lesion may be bypassed by inserting, generally, deoxyadenosine opposite the lesion (*6*, *7*). To protect genome integrity, living organisms have robust enzyme activities, mainly Exonuclease III in bacteria and Ape1 in mammalian cells, that recognize the lesion and cut the DNA backbone 5′ to the AP site, initiating the repair process (*8*−*10*). The continuous generation and repair of AP sites results in a steady-state level that, depending on the tissue analyzed and isolation procedures, has been estimated to be between 50 000 and 200 000 lesions per cell (*11*, *12*).

Abasic sites in DNA induce a significant reduction of the duplex thermodynamic stability. The magnitude of this effect varies largely with DNA sequence, being highly affected by the base pairs flanking the lesion but only marginally influenced by the identity of the orphan base (*13*, *14*). The AP site exists as an interconverting mixture of α-2′-deoxy-D-ribose, β-2′-deoxy-D-ribose, and a small percentage of the open forms, namely, the aldehyde and its hydrated form (Scheme 1). This equilibrium process (also known as mutarotation) increases the instability of the abasic site because the open aldehydic form is the actual substrate for the β- and β−δ-elimination reactions mediated by DNA glycosylases that results in a single-strand break (*15*).

Several solution structures of DNA duplexes containing natural and modified AP sites have been determined using NMR spectroscopy. Despite the large reduction in thermodynamic stability, DNA duplexes that contain AP sites show, with few exceptions, small distortions on the sugar−phosphate backbone, which maintain approximately a B-form conformation (*16*−*28*). Local perturbations of the DNA structure are largely dependent on the sequence context surrounding the lesion and, contrary to the thermodynamic results, on the identity of the orphan residue. When AP sites

[†] NIH Grants CA47995 and CA093502 supported this research.

[‡] Atom coordinates have been deposited in the Protein Data Bank as entries 1XCY and 1XCZ for the α-carba- and β-carba-AP duplexes, respectively.

* To whom correspondence should be addressed. Telephone: (631) 444-3649. Fax: (631) 444-3218. E-mail: cds@pharm.sunysb.edu.

[1] Abbreviations: NMR, nuclear magnetic resonance; PAGE, polyacrylamide gel electrophoresis; EDTA, disodium ethylenediamine tetraacetate; NOESY, nuclear Overhauser effect spectroscopy; COSY, correlation spectroscopy; DQF-COSY, double-quantum-filtered correlation spectroscopy; TOCSY, homonuclear Hartmann−Hahn spectroscopy; NOE, nuclear Overhauser effect; HPLC, high-performance liquid chromatography; MD, molecular dynamics; rmsd, root-mean-square deviation; AP, apurinic/apyrimidinic; Ape, apurinic (apyrimidinic) endonuclease.

10.1021/bi048400c CCC: $27.50
Published on Web 11/16/2004

Scheme 1: Isomeric Exchange of Naturally Occurring Abasic Sites[a]

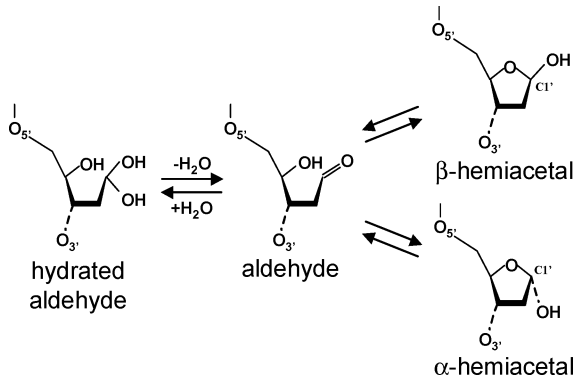

[a] At equilibrium, the hemiacetal forms make up 98% of the sample.

Scheme 2: Structure of Carbocyclic Abasic Sites (top) and Duplex Sequence Used in This Study (bottom)

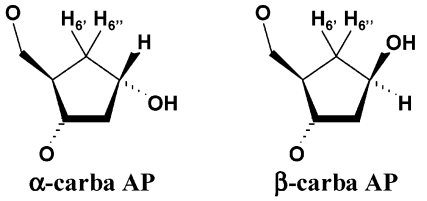

C1 G2 T3 A4 C5 X6 C7 A8 T9 G10 C11
G22 C21 A20 T19 G18 A17 G16 T15 A14 C13 G12

are opposite a pyrimidine base (apurinic sites), the duplex structure has increased conformational flexibility at the lesion site. Depending on experimental conditions and sequence context, the structure may have the AP site and its partner base inside the helix (*22*−*25*), or have both residues completely on the outside of the helix (*17*), or alternatively, only the orphan residue may be in the extrahelical position (*17*, *26*). When the AP site pairs to purine bases (apyrimidinic sites), the opposing residue is always inside the duplex and the lesion may remain intra- or extrahelical, depending on the sequence context and the nature of the abasic site used for the study (*16*−*21*, *25*, *27*, *28*). Duplex structures determined using tetrahydrofuran residues, a stable AP site analogue with a hydrogen atom in place of the C1′ OH group (Scheme 1), always have the lesion in an intrahelical conformation (*16*−*18*). In contrast, structural studies performed using the natural AP site show that the lesion can adopt a large number of different conformations. Depending on the sequence context, the α- and *β*-anomers of the lesion may stay inside the duplex (*20*, *25*), or both forms may adopt an extrahelical conformation (*28*). Alternatively, only the α-anomer may be external to the helix, and this induces a large structural perturbation (*21*, *27*).

To understand further the role played by the C1′ OH group in local duplex structure, we have designed carbocyclic abasic site analogues (carba-AP site) of the natural lesion (Scheme 2), which carry a methylene substitution at the ribose O4′ position, thus eliminating the process of mutarotation. Here we report the NMR solution structure of two 11-mer oligodeoxynucleotide duplexes containing the α- or *β*-anomer of the carba-AP site with dA as the counter base. The numbering and sequence of the duplexes used in our studies are shown in Scheme 2.

Scheme 3: Synthesis of Carbocyclic Abasic Site Precursors for Solid-Phase Synthesis[a]

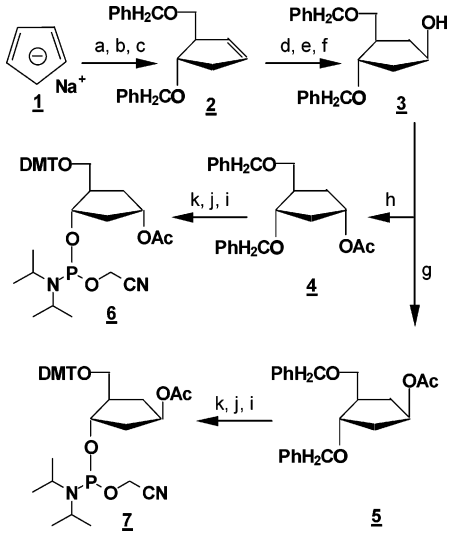

[a] (a) $PhCH_2OCH_2Cl$; (b) (−)-Ipc_2BH followed by NaOH, H_2O_2; (c) NaH, $PhCH_2Cl$; (d) PhSeCl, AgO_2CCF_3; (e) 5% KOH in ethanol; (f) Ni-Raney; (g) Ac_2 in pyridine; (h) DEAD/Ph_3P/AcOH in THF; (i) 10% Pd over carbon; (j) DMT-Cl in pyridine; (k) *β*-cyanoethylphosphoramidite-Cl in TEA.

EXPERIMENTAL PROCEDURES

Synthesis of Carba-AP Sites. The synthesis of the two DMT-phosphoramidites needed for the preparation of the oligodeoxynucleotide samples is shown in Scheme 3. The key intermediate, namely, compound **3**, was obtained using a variation of the selenium chemistry developed by Marquez and co-workers, which delivers the requisite compound **3** in a stereo- and chemoselective fashion (*29*). Compound **3** was smoothly converted into **4**, which contains the inverted stereochemistry at the pseudoanomeric carbon, by employing the Mitsunobu conditions with acetic acid serving as the nucleophilic component (*30*). Dibenzylic compounds **4** and **5** were subsequently transformed into their DMT-phosphoramidites **6** and **7**, respectively, using standard nucleoside chemistry protocols. The proton NMR spectrum of compound **3** in $CDCl_3$ at 250 MHz shows signals at 7.38−7.25 (m, 10H), 4.53−4.47 (m, 4H), 4.33−4.30 (m, 1H), 4.09−4.04 (m, 1H), 3.54−3.51 (m, 2H), 2.76 (bs, 1H), 2.34−2.26 (m, 1H), 2.05−2.01 (m, 1H), 1.92−1.85 (m, 1H), and 1.52−1.47 ppm (m, 1H). The $\{^1H\}^{13}C$ NMR spectrum of compound **3** in $CDCl_3$ at 62.5 MHz shows signals at 138.54, 137.76, 128.25, 127.66, 81.79, 72.07, 72.00, 71.26, 44.00, 42.44, and 37.84 ppm. The FAB mass spectrum shows an $(M + H)^+$ of 313.1 Da.

Sample Preparation. Unmodified and lesion-containing oligodeoxynucleotides were synthesized using standard chemistry methods. DNA sequences containing a 5′-dimethoxytrityl group were cleaved from the solid support by treatment of the crude synthetic products with concentrated aqueous ammonia for 46 h at room temperature. Purification of the oligodeoxynucleotides was accomplished by reverse-phase HPLC using a preparative Dynamax (300 mm × 25 mm) C4 column. The mobile phase consisted of solvent A [0.1 M triethylammonium acetate buffer (pH 7.0)] and solvent B (acetonitrile). Using a linear gradient from 0 to 50% B over the course of 50 min, the main fraction

containing the desired compound was eluted around 33 min. After lyophilization of the main HPLC fraction, the terminal DMT group was cleaved by treatment with an 80% acetic acid solution for 30 min and the solution extracted with ether three times prior to a second round of purification by HPLC. After HPLC purification, the composition of each oligomer was confirmed by electrospray mass spectrometry. Oligodeoxynucleotides used for NMR studies were desalted using a Sephadex G-25 column and converted to the sodium salt by percolation through a Dowex 50W cation exchange resin. Annealing of duplex samples was achieved by mixing the appropriate amounts of each strand in an aqueous solution (estimated using the ϵ_{260} computed by Gene Runner version 3.0, Hasting Softwarte, Inc.) and then heating the mixture to 95 °C followed by slow cooling to room temperature. NMR samples consisted of 1.2 mmol of duplex dissolved in 0.7 mL of 50 mM phosphate buffer (pH 6.9) containing 50 mM NaCl and 1 mM EDTA, using either 99.96% D_2O or a 90% H_2O/10% D_2O mixture (v/v). Samples were vacuum-degassed inside the NMR tube prior to data collection.

Synthesis of oligodeoxynucleotides employed to assay Ape1 incision at carba-AP sites followed similar procedures. Duplex samples used in these experiments contained, internally, the sequence employed for structural studies (underlined residues), namely, d(CGTCACCGTACXCATGCTGCACATCC)·d(GGATGTGCAGCATGAGTACGGTGACG) (X is an α-carba-AP residue, a *β*-carba-AP residue, or a tetrahydrofuran AP residue). Incision reaction mixtures contained DNA substrate (100 nM) and recombinant Ape1 (0.03 nM), dissolved in a buffer solution [50 mM HEPES (pH 7.5)] containing 50 mM KCl, 1 *μ*g/mL BSA, 10 mM $MgCl_2$, and 0.5% Triton X-100. Reaction mixtures were incubated at 37 °C during the indicated period of time and reactions terminated by the addition of a 95% $HCOONH_2$ solution containing 20 mM EDTA followed by heating at 95 °C for 10 min. Analysis was accomplished by 12% PAGE in the presence of 7 M urea.

NMR Experiments. One- and two-dimensional experiments were carried out using high-field spectrometers operating at field strengths of 11.75 and 14.1 T. Proton chemical shifts were referenced relative to sodium 3-(trimethylsilyl)propionate-2,2,3,3-d_4. Phase-sensitive (*31*) NOESY (mixing times of 50, 120, 180, and 300 ms), TOCSY (mixing times of 70 and 140 ms), COSY, DQF-COSY, and COSY45 spectra in 100% D_2O buffer were recorded at 17 °C using a repetition time of 1.5 s, during which the residual water signal was suppressed by saturation. Phase-sensitive proton NOESY (mixing times of 120 and 220 ms) spectra in 90% H_2O buffer were recorded at 4 °C for both samples, using a jump and return reading pulse (*32*). Time domain data sets consisted of 2048 and 300 complex data points in the t_2 and t_1 dimensions, respectively. COSY45 spectra, acquired with twice the number of complex points in the t_2 dimension, were used to evaluate deoxyribose conformations on each duplex. Phase-sensitive $^1H-^{31}P$ HETCOR spectra in 100% D_2O buffer were recorded with 2048 and 128 complex data points in the t_2 and t_1 dimensions, respectively, using the indirect detection mode (*33*). Phosphorus chemical shifts were referenced to external TMP. All NMR data were processed and analyzed using Felix (Accelrys Inc., San Diego, CA) running on Silicon Graphics computers. Time domain data were multiplied by 90°-shifted sine bell window functions prior to Fourier transformation. No baseline corrections were applied to the transformed spectra.

Structural Refinement. Interproton distance calculation and molecular dynamics simulations were carried out using XPLOR3.85 on Silicon Graphics workstations (*34*). Distances were computed by subjecting a canonical B-form duplex structure to energy minimization, using only a "relax" potential energy function (*35*), which was proportional to the differences between back-calculated and experimental NOE intensities, measured from all NOESY spectra. Prior to the minimization, a grid search revealed that a value of 1.95 ns was the best-fit isotropic correlation time. Molecular dynamics simulations were performed *in vacuo* using a CHARMM-derived force field (*36*), phosphate charges set to −1, and a dielectric constant value of 4 (*37*). A total of 389 interproton distances for the α-carba-AP duplex and 400 for the *β*-carba-AP duplex were restrained during molecular dynamics using square-well potential energy functions. Reflecting the quality of experimental data, distance bounds of ±0.6 and ±0.9 Å of the back-calculated value were used on distances derived from nonoverlapping peaks and of ±1.5 Å on those derived from overlapping peaks. Watson−Crick alignments were enforced using square-well potential energy functions, with equilibrium hydrogen bond distances taken from crystallographic studies and bounds of ±0.1 Å. On the basis of COSY45 data, sugar conformations were enforced within the C2′-*endo* range using empirical dihedral angle potential energy functions (*38*, *39*). Similarly, backbone dihedral angles were enforced in a range encompassing A- and B-form DNA conformations. Canonical B-form starting structures of each duplex were generated in InsightII (Accelrys). Molecular dynamics consisted of a heating step, where the temperature of the system increased from its initial value to 500 K in 70 ps, followed by a high-temperature step, during which the simulation remained at 500 K for different periods of time (42, 44, 46, 48, and 50 ps). After completion of the high-temperature step, the system was cooled to 300 K over a period of 70 ps and equilibrated at this temperature for an additional 125 ps. Experimental distance bounds were enforced with a force constant of 100 kcal mol^{-1} $Å^{-2}$ for heating stage and high-temperature steps and 50 kcal mol^{-1} $Å^{-2}$ for the cooling and equilibration steps. A total of 20 distance-restrained structures were calculated for each duplex by starting the simulation from four different initial temperatures (100, 150, 200, and 250 K) and five variations in the length of the high-temperature step. The last coordinate frame of the simulations was energy-minimized, generating the refined structures. Nine refined structures for each duplex, having a pairwise rmsd of <1.4 Å, comprised the final ensemble of structures presented here. Analysis of structural parameters was performed with Curves (*40*).

RESULTS

NMR Characterization of Duplexes Containing Carbocyclic AP Sites. One-dimensional spectra of the α- and *β*-carba-AP duplexes recorded in 100% D_2O buffer (pH 6.8) at 17 °C exhibit sharp proton signals, suggesting the existence of a main average conformation in solution (Figure 1S of the Supporting Information). Assignment of the nonexchangeable base and sugar protons follows the analysis of

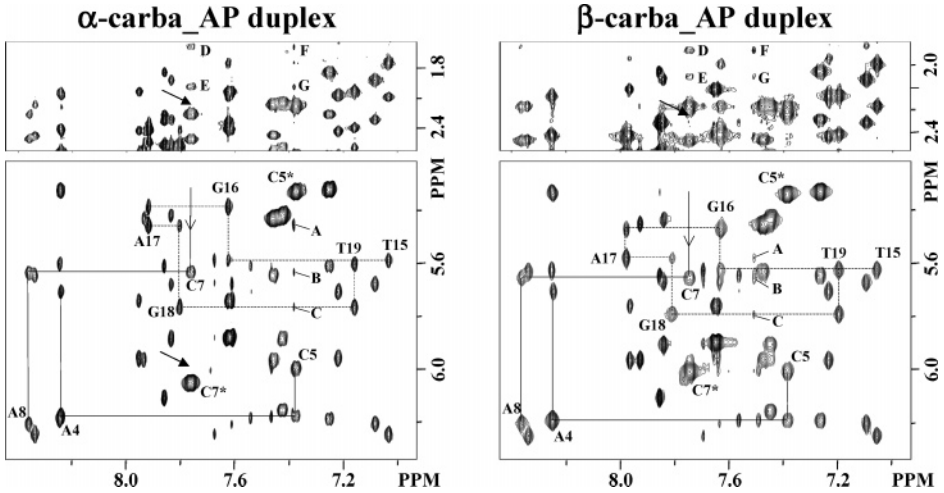

FIGURE 1: Expanded contour plots of NOESY (mixing time of 300 ms) spectra recorded in 50 mM phosphate buffer at pH 6.8 and 17 °C depicting interactions between base (purine H8/pyrimidine H6) and sugar H1′, H2′, and H2″ protons of carba-AP duplexes. Labels identified intraresidue cross-peaks between the base and H1′ sugar protons, drawn only for the central segment of the duplexes. Black arrows point to the absence of NOE peaks between C5 and C7 residues. Other labels are assigned as follows: (A) A17 H2−A17 H1′, (B) A17 H2−C7 H1′, (C) A17 H2−G18 H1′, (D) C7 H6−AP H2″, (E) C7 H6−AP H2′, (F) A17 H2−AP H2″, and (G) A17 H2−AP H2′. Asterisks indicate cytosine H5−H6 NOE cross-peaks.

NOESY, COSY, and TOCSY spectra using established procedures (*41*, *42*). As shown in Figure 1, sequential NOE interactions throughout both duplexes correlate each base proton (purine H8 or pyrimidine H6) with the H1′ proton of its own as well as that of the 5′-flanking deoxyribose. As expected, the presence of the carba-AP residues disrupts these interactions at the C5/AP6 step in both duplexes. Furthermore, in the 50 ms mixing time NOESY spectrum, the intensities of the intraresidue base−H1′ cross-peaks are weak, suggesting that all nucleotides have their *N*-glycosidic torsion angle in the *anti* range. In the case of the α-carba-AP duplex, the spectrum lacks NOE interactions between C7 H6 (or C7H5) and the H1′, H2′, H2″ (Figure 1, black arrows), or H3′ (not shown) sugar protons of C5, suggesting a separation of more than 5 Å between these residues. A similar observation for the *β*-carba-AP duplex is partially hindered by signal overlap. However, the absence of C7 H6−C5 H2″ (Figure 1, black arrow) and C7 H6−C5 H3′ (not shown) cross-peaks suggests a wide separation between these two residues in the *β*−carba-AP duplex. In addition, the spectra show weak but clear NOE interactions between A17 H2 and the H1′ protons of A17, G18, and C7 (Figure 1, peaks A, C, and B, respectively), indicating short distances among these protons in both duplexes. Furthermore, A17 H2 also shows NOE peaks to the H1′ (not shown), H2′, and H2″ protons of the AP residue (Figure 1, peaks G and F, respectively), establishing short distances among protons across the lesion-containing pair.

One-dimensional phosphorus spectra of the α- and *β*-carba-AP duplexes recorded in 100% D_2O buffer at 17 °C exhibit partially resolved signals with one phosphate resonance, subsequently assigned to the carbocyclic AP residues, resonating ∼0.7 ppm downfield from all other signals (Figure 2S of the Supporting Information). A downfield-shifted phosphorus signal has been observed frequently in the spectra of duplexes containing a natural abasic site, a deoxyribonolactone abasic site, and in the spectra of several abasic site analogues (*18*−*20*, *23*−*25*, *27*), suggesting that the novel carbocyclic AP site does not cause additional perturbations of the phosphodiester backbone. Proton and phosphorus chemical shifts of α-AP and *β*-AP duplexes are listed in Tables 1S and 2S of the Supporting Information, respectively.

Assignment of carba-AP protons follows the analysis of regions of the COSY spectra shown in Figure 3S of the Supporting Information, which are mostly devoid of 2′-deoxyribose signals. Signals of the H1′, H3′, H5′, and H5″ protons, which are geminal to oxygen atoms, resonate between 3.6 and 4.4 ppm, while those of H2′, H2″, H4′, H6′, and H6″ protons appear upfield in the range of 1.5−2.4 ppm. The H5′ and H5″ signals are readily identified because they show COSY peaks to the H4′ proton only. In contrast, H3′ exhibits three cross-peaks, namely, to the H2′, H2″, and H4′ protons, and H1′ shows four COSY peaks, to the H2′, H2″, H6′, and H6″ protons (Figure 2S of the Supporting Information). The stereospecific assignment of carba-AP H2′ and H2″ protons follows the intensity evaluation of their NOE peaks to the H1′ proton in a short mixing time (120 ms) NOESY spectrum. Independent of the sugar conformation, the H1′−H2″ distance is shorter than the H1′−H2′ distance, and thus, the H1′−H2″ NOE cross-peak is always stronger than the H1′−H2′ one at short mixing times. Similarly, NOE peak intensities to the H4′ proton differentiate between the carba-AP H6′ and H6″ proton signals, and the H5′ and H5″ protons are not stereospecifically assigned. Proton chemical shifts of the α- and *β*-AP residues are listed in Tables 1S and 2S of the Supporting Information, respectively.

Figure 2 displays the imino proton region of one-dimensional spectra of carba-AP duplexes recorded in 10% D_2O buffer solutions at 4 °C. The spectra are very similar with seven well-resolved signals between 12.0 and 14.0 ppm accounting for all imino protons of both duplexes. The variation of the imino proton signals with temperature, shown in Figure 4S of the Supporting Information, indicates that both duplexes have similar thermal stability with a melting temperature of ∼40 °C. Assignment of the exchangeable protons follows the analysis of NOESY (mixing time of 220 ms) spectra recorded at low temperatures (*41*, *42*). As shown in Figure 2, each thymine imino proton shows strong NOE interactions to their corresponding adenine H2 proton across

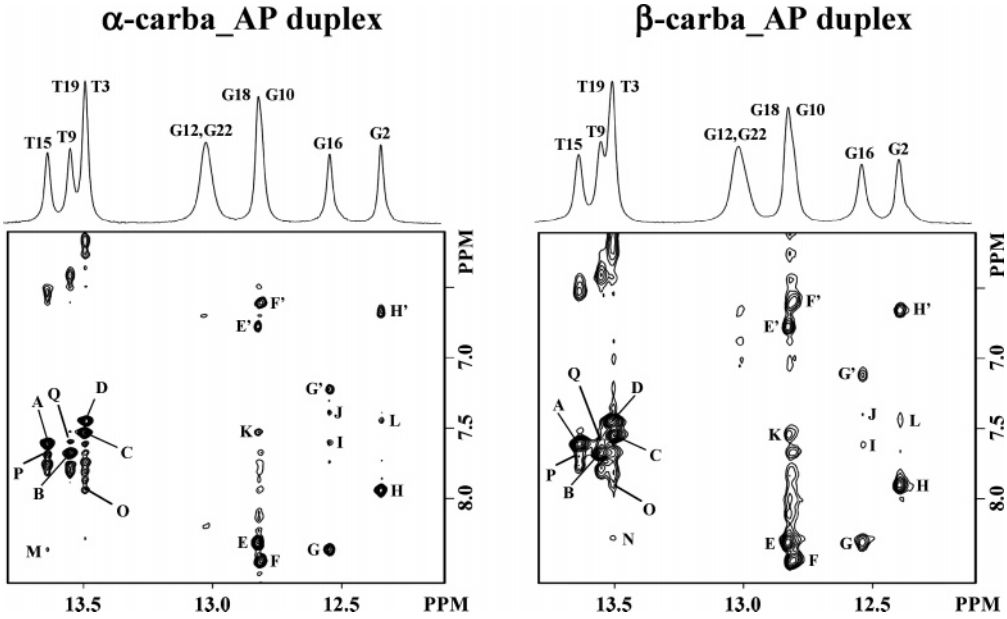

FIGURE 2: Expanded contour plots of NOESY (mixing time of 220 ms) spectra recorded in 50 mM phosphate buffer at pH 6.8 and 4 °C showing interactions between the imino and base/amino proton regions of carba-AP duplexes. Labels are assigned as follows: (A) T15 N3H−A8 H2, (B) T9 N3H−A14 H2, (C) T19 N3H−A4 H2, (D) T3 N3H−A20 H2, (E/E′) G18 N1H−C5 N4H_{HB}/G18 N1H−C5 N4H_{nHB}, (F/F′) G10 N1H−C13 N4H_{HB}/G10 N1H−C13 H_{nHB}, (G/G′) G16 N1H−C7 N4H_{HB}/G16 N1H−C7 N4H_{nHB}, (H/H′) G2 N1H−C21 N4H_{HB}/G2 N1H−C21 N4H_{nHB}, (I) G16 N1H−A8 H2, (J) G16 N1H−A17 H2, (K) G18 N1H−A4 H2, (L) G2 N1H−A20 H2, (M) T15 N3H−C7 N4H_{HB}, (N) T19 N3H−C5 N4H_{HB}, (O) T3 N3H−C21 N4H_{HB}, (P) T15 N3H−A14 H2, and (Q) T19 N3H−A8 H2. HB and nHB refer to the hydrogen-bonded and non-hydrogen-bonded amino protons, respectively.

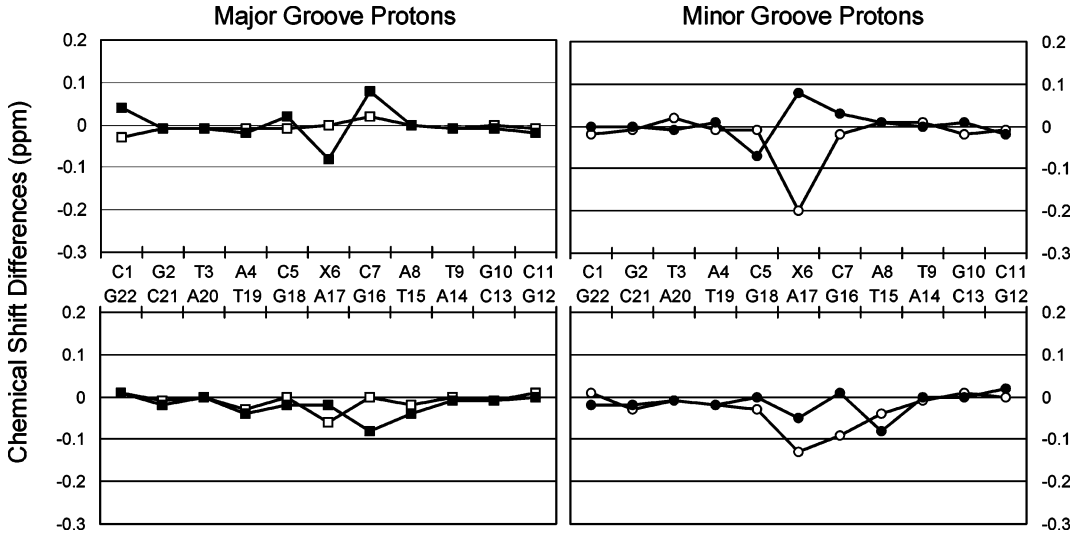

FIGURE 3: Chemical shift differences between carba-AP duplexes measured in 50 mM phosphate buffer at pH 6.8 and 17 °C. Graphed differences are α-carba-AP minus *β*-carba-AP chemical shifts for the major groove (□) base (purine H8/pyrimidine H6) and (■) sugar H2′ protons and for the minor groove sugar (○) H1′ and (●) H2″ protons. Chemical shift differences for the H6′ and H6″ protons of the carba-AP residues are 0.39 and −0.38 ppm, respectively.

the base pair (Figure 2, peaks A−D). Similarly, with the exception of the terminal base pairs, guanine imino protons show strong NOE cross-peaks to the amino protons of their counter cytosine partners (Figure 2, peaks E/E′−H/H′). Figure 2 also shows weak sequential connectivities between guanine imino and adenine H2 protons (Figure 2, peaks I−L), including a clear G16 N1H−A17 H2 NOE peak in both duplexes (Figure 2, peak J), indicating that A17, partner of the AP residues, is intrahelical. Likewise, thymine imino protons display sequential NOE peaks to some of the cytosine amino protons and to the adenine H2 protons in the A8·T15-T9·A14 step (Figure 2, peaks M−O and P and Q, respectively). Furthermore, the spectra reveal NOE interactions between sequential imino protons, interrupted only at the lesion site (Figure 5S of the Supporting Information), suggesting normal base pair stacking throughout both duplexes. The chemical shifts of exchangeable protons are listed in Tables 1S and 2S of the Supporting Information.

Assignment of proton signals permits the observation of chemical shift differences between homologous protons of carba-AP duplexes which, in principle, may result from the C1′ configuration of the AP site or be due to different solution structures adopted by the duplexes. As shown in Figure 3, proton chemical shifts external to the lesion site are mostly identical, thus establishing the lack of global structural differences between the duplexes. At the lesion

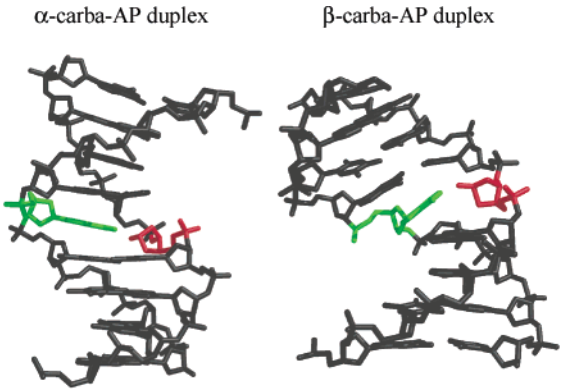

FIGURE 4: Refined three-dimensional structures of α-carba-AP (left) and *β*-carba-AP (right) duplexes, seen with the major groove prominent. Only heavy atoms are shown, with carba-AP lesions colored red, their adenosine partners green, and all other residues gray.

site, the H2′, H2″, H1′, H6′, and H6″ protons of the carba-AP residues show the largest chemical shift differences. The fact that chemical shift differences between H2′ and H2″ have opposite signs suggests that they originate from the configuration of C1′, in which the oxygen atom at this position is close to only one proton of the vicinal methylene group. The chemical shift differences between the H6′ and H6″ protons of the duplexes follow an identical pattern. Of the bases that flank the lesion site, proton chemical shift differences for the C5·G18 pairs are not significant and those for the C7·G16 pair are minor and reflect the proximity of the 1′-oxygen of the abasic site, the latter being brought about by the right-handedness of the duplex. Among exchangeable protons, only the amino protons of C7 show small but significant chemical shift differences.

Three-Dimensional Structures. Distance-restrained molecular dynamics generated a series of three-dimensional models in excellent agreement with the experimental NMR data. Figure 6S of the Supporting Information displays overlap views of the converging models, and Figure 4 shows a representative structure of each duplex. As can be seen in the figures, the presence of the AP site does not cause large deviations from the canonical B-form DNA structure. Independent of the AP site C1′ configuration, the abasic residues and their adenine partners are intrahelical. Both duplexes are right-handed helices with glycosidic torsion angles in the *anti* orientation for all residues and sugar conformations in the C2′-*endo*/C3′-*exo* range. The structure of the *β*-carba-AP duplex shows more flexibility, and in some of the converging models, the deoxyriboses of lesion-flanking residues assume a conformation within the C1′-*exo* range. In the α-carba-AP duplex, all base pairs adopt Watson−Crick alignments and show appropriate base stacking throughout the duplex, which is interrupted at the lesion site by the presence of the abasic residue. Similarly, the *β*-carba-AP duplex shows Watson−Crick alignments on all canonical base pairs, but stacking is disrupted not only by the presence of the abasic site residue but also by a kink in the direction of the major groove at the A17-G18 step.

Figure 5 shows close-up views of the lesion sites and depicts small structural differences between the duplexes. Base pairs flanking the lesion are appropriately hydrogen bonded, and in the case of the *β*-carba-AP duplex, the C7·G16 pair shows a slight buckle. Independent of its

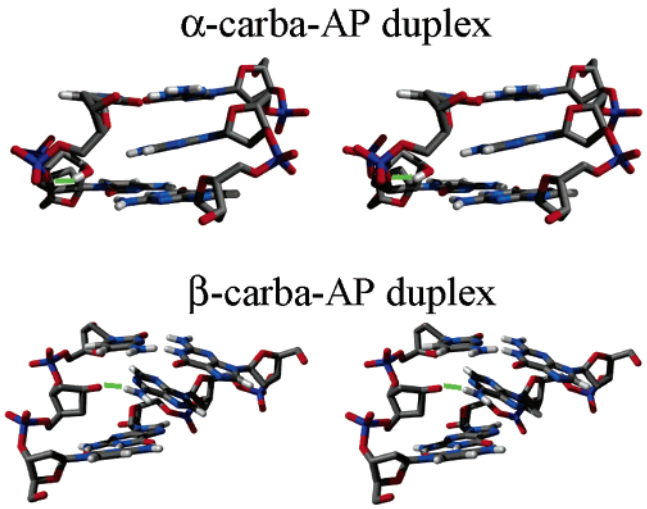

FIGURE 5: Cross-eye stereo representation of lesion site structures, showing the minor groove prominent on the α-carba-AP duplex, the major groove prominent on the *β*-carba-AP duplex, and atoms colored by type. The green lines represent C1′ configuration-dependent hydrogen bonds formed by the carbocyclic abasic site.

Table 1: Structure Calculations

	α-carba-AP duplex	*β*-carba-AP duplex
deviations from experimental restraints[a]		
rmsd for NOE distances[b] (Å)	0.019	0.017
NOE energy[b] (kcal mol^{-1} Å^{-2})	34 ± 2	24 ± 2
van der Waals energy (kcal/mol)	−329 ± 2	−324 ± 2
rmsd from idealized geometry[a]		
bond lengths (Å)	0.016	0.013
bond angles (deg)	4.2	3.9
improper angles (deg)	0.17	0.19

[a] Measured on each of the final refined structures. [b] Average values determined on distance-refined structures. A total of 265 experimental distances.

configuration, the C1′ OH group participates in hydrogen bonding. In the case of the α-isomer, seven of the nine converging structures show intraresidue hydrogen bonding between C1′ OH and O3′ groups, whereas in the other two, the C1′ OH groups is hydrogen bonded to the ring O4′ of the flanking C7 residue. In the case of the *β*-isomer, the AP site C1′ oxygen forms an interstrand hydrogen bond with one of the amino protons of its partner A17 residue, in six of the nine converging structures. An additional structural feature that depends on the C1′ configuration of the AP site is the value of glycosidic torsion angles adopted by flanking cytidine residues. In the case of the α-isomer, *χ* torsion angles of C5 are in the *high-anti* range, whereas those of C7 are slightly higher, adopting unusual *syn* values. On the other hand in the *β*-AP duplex, *χ* torsion angles of C7 are now in the normal *high-anti* range, whereas those of C5 are slightly inside the *syn* range. Independent of the C1′ configuration of the abasic lesion, the glycosidic torsion angles of residues on the unmodified strand are in the *high-anti* range. Statistics of the refinement and values of the relevant structural parameters are listed in Table 1.

Ape1 Incision of Carba-AP Sites. Figure 6 shows PAGE analysis of reaction mixtures after incubation of AP site-containing duplexes with human Ape1. The result indicates that Ape1 can incise DNA duplexes containing either isomer of the carbocyclic AP site analogue, indicating that the

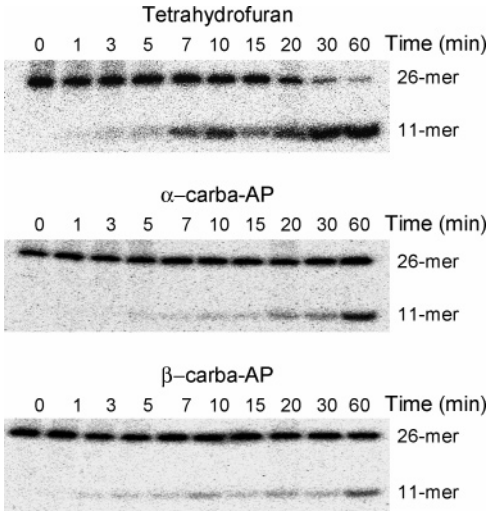

FIGURE 6: Time dependence of Ape1 incision of DNA duplexes containing abasic site analogues. PAGE analysis indicates that, while the Ape1 is more active nicking DNA with a tetrahydrofuran residue, it shows similar activity on α- and *β*-carbocyclic AP sites.

endocyclic sugar oxygen is not required for enzyme activity. In addition, whereas Ape1 is more active in nicking duplexes containing a tetrahydrofuran AP site, the extent of enzyme incision for both isomers of the carbocyclic AP sites is similar, indicating that the configuration at the C1′ position of the lesion makes no difference in enzyme processing.

DISCUSSION

The main motivation for this study was to establish what, if any, global and/or local structural changes are induced by the C1′ α- and *β*-isomers of AP sites in double-stranded DNA duplexes. To this end, the newly designed carbocyclic AP site analogue offers the advantage of preventing interconversion between the isomeric forms of the lesion, thus simplifying the analysis and interpretation of the results. Our experimental data indicate that the configuration of the C1′ hydroxyl group of the AP site does not influence the global structure of duplex DNA. Chemical shift differences between equivalent duplex protons are significant only at and near the lesion, indicating that any structural difference induced by isomerism at the C1′ OH position of the lesion is purely local. This fact is not surprising considering that only local structural perturbations have been reported previously when a natural AP site is incorporated into DNA duplexes lacking A-tract sequences (*20*, *21*, *25*, *28*).

At the lesion site, carba-AP residues and their dA partners are positioned inside the helix. The intrahelical character of orphan purine residues has been consistently observed in studies using both the natural AP site (*20*, *21*, *25*, *27*, *28*) and its tetrahydrofuran analogue (*16*−*18*). In contrast, the presence of either of the carba-AP sites inside the helix adds to the conflicting results previously observed with natural lesions (*20*, *21*, *25*, *28*). One possibility is that lesion-flanking base pairs may influence the helical character of AP sites. The duplex studied in this report has the AP site flanked by C·G pairs, nominally the most stable sequence, a context that would reduce dynamics at the lesion site and favor an intrahelical position. Refined structures of a natural AP site flanked by C·G pairs have not been reported, but their NMR characteristics imply an intrahelical location for the AP lesion (*20*). However, AP sites are extrahelical when flanked by C·G and T·A pairs (*28*) or may adopt isomer-dependent conformations when A·T pairs, supposedly the least stabilizing situation, are neighbors of the lesion (*21*, *25*). Taken together, these results suggest that the helical location of AP lesions may be influenced by, although not directly correlated with, the stability of flanking base pairs.

Local structural differences induced in duplex DNA by the configuration of the anomeric carbon are only minor. Molecular dynamics simulations run in the absence of explicit solvent molecules showed that hydrogen bonds formed by the AP residue are different for each isomer (Figure 5). In the case of the α-isomer, the C1′ OH group acts as a hydrogen donor, forming a hydrogen bond with oxygen acceptors located in the same strand of the duplex, namely, O3′ of the AP lesion or O4′ of the flanking C7 residue. In contrast, the C1′ OH group of the *β*-isomer forms an interstrand hydrogen bond acting as an acceptor for one of the amino protons of its partner A17 residue. However, the additional interstrand hydrogen bond present in the case of the *β*-carba-AP isomer did not increase the thermal stability of the DNA in any significant manner, because both duplexes exhibit similar NMR melting temperatures (Figure 4S of the Supporting Information). The failure to detect increased stability for the *β*-carba-AP duplex suggests that structured water molecules form additional hydrogen bonds at the lesion site, leveling the melting temperatures of both duplexes.

On the basis of the X-ray structure of an Ape1−DNA complex, it has been postulated that the enzyme recognizes and cleaves exclusively the α-isomer of the AP lesion because in its *β*-configuration the C1′ OH group could not be accommodated in the hydrophobic active site pocket (*43*). Our results from DNA incision assays clearly rebut this hypothesis and show that Ape1 recognizes and cleaves α- and *β*-AP sites with identical efficiency. Furthermore, Ape1 kinetic parameters for duplexes containing α-carba- and *β*-carba-AP isomers, namely, K_m, K_{cat}, and V_{max}, are essentially indistinguishable individually, and bacterial Fpg protein, which also recognizes abasic sites in DNA, binds both isomers with similar affinity (manuscript in preparation). Thus, it is highly likely that the configuration of the hydroxyl group at C1′ of natural AP sites is inconsequential for their processing by human Ape1, bacterial Fpg, and, probably, other base excision repair proteins. However, as the crystal structure suggests, the active site of Ape1 needs to adjust not only to the C1′ configuration of the natural AP site but also to several other types of residues lacking a base that are incised with similar efficiency (*44*). It would be of great interest to understand the structural mechanisms that facilitate the active site plasticity of Ape1 and, on a broader perspective, of BER proteins, which frequently show broad substrate specificity.

ACKNOWLEDGMENT

We thank Ms. Cecilia Torres for the synthesis and purification of oligodeoxynucleotides.

SUPPORTING INFORMATION AVAILABLE

Tables 1S and 2S listing proton and phosphorus chemical shifts of the α-carba- and *β*-carba-AP duplexes, respectively.

Figures showing one-dimensional nonexchangeable proton spectra (Figure 1S), one-dimensional phosphorus spectra (Figure 2S), the temperature dependence of the exchangeable protons (Figure 4S), expanded regions of a COSY spectrum depicting interactions among carba-AP protons (Figure 3S), expanded regions of a NOESY spectrum depicting interactions among the imino protons (Figure 5S), and an overlap view of converging duplex structures (Figure 6S). This material is available free of charge via the Internet at http://pubs.acs.org.

REFERENCES

1. Lindahl, T., and Nyberg, B. (1972) Rate of Depurination of Native Deoxyribonucleic Acid, *Biochemistry 11*, 3610−3618.
2. Nakamura, J., Walker, V. E., Upton, P. B., Chiang, S. Y., Kow, Y. W., and Swenberg, J. A. (1998) Highly Sensitive Apurinic/apyrimidinic Site Assay Can Detect Spontaneous and Chemically Induced Depurination under Physiological Conditions, *Cancer Res. 58*, 222−225.
3. Loeb, L. A., and Preston, B. D. (1986) Mutagenesis by apurinic/apyrimidinic sites, *Annu. Rev. Genet. 20*, 201−230.
4. Kusmierek, J. T., Folkman, W., and Singer, B. (1989) Synthesis of N2,3-ethenodeoxyguanosine, N2,3-ethenodeoxyguanosine 5′-phosphate, and N2,3-ethenodeoxyguanosine 5′-triphosphate. Stability of the Glycosyl Bond in the Monomer and in Poly(dG,ϵdG-dC), *Chem. Res. Toxicol. 2*, 230−233.
5. Friedberg, E. C., Walker, G. C., and Siede, W. (1995) in *DNA Repair and Mutagenesis*, ASM Press, Washington, DC.
6. Strauss, B. S. (1991) The "A" Rule of Mutagen Specificity: A Consequence of DNA Polymerase Bypass of Non-Instructional Lesions? *BioEssays 13*, 79−84.
7. Zou, W., and Doetsch, P. W. (1993) Effects of Abasic Sites and DNA Single-Strand Breaks on Prokaryotic RNA Polymerases, *Proc. Natl. Acad. Sci. U.S.A. 90*, 6601−6605.
8. Weiss, B. (1976) Endonuclease II of *Escherichia coli* is exonuclease III, *J. Biol. Chem. 251*, 1896−1901.
9. Robson, C. N., and Hickson, I. D. (1991) Isolation nf cDNA Clones Encoding a Human Apurinic/Apyrimidinic Endonuclease that Corrects DNA Repair and Mutagenesis Defects in *E. coli* xth (Exonuclease III) Mutants, *Nucleic Acids Res. 19*, 5519−5523.
10. Demple, B., Herman, T., and Chen, D. S. (1991) Cloning and Expression of APE, the cDNA Encoding the Major Human Apurinic Endonuclease: Definition of a Family of DNA Repair Enzymes, *Proc. Natl. Acad. Sci. U.S.A. 88*, 11450−11454.
11. Nakamura, J., and Swenberg, J. A. (1999) Endogenous Apurinic/Apyrimidinic Sites in Genomic DNA of Mammalian Tissues, *Cancer Res. 59*, 2522−2526.
12. Atamna, H., Cheung, I., and Ames, B. N. (2000) A Method for Detecting Abasic Sites in Living Cells: Age-Dependent Changes in Base Excision Repair, *Proc. Natl. Acad. Sci. U.S.A. 97*, 686−691.
13. Gelfand, C. A., Plum, G. E., Grollman, A. P., Johnson, F., and Breslauer, K. J. (1998) Thermodynamic consequences of an abasic lesion in duplex DNA are strongly dependent on base sequence, *Biochemistry 37*, 7321−7327.
14. Ide, H., Shimizu, H., Kimura, Y., Sakamoto, S., Makino, K., Glackin, M., Wallace, S. S., Nakamuta, H., Sasaki, M., and Sugimoto, N. (1995) Influence of α-Deoxyadenosine on the Stability and Structure of DNA. Thermodynamic and Molecular Mechanics Studies, *Biochemistry 34*, 6947−6955.
15. Bhagwat, M., and Gerlt, J. A. (1996) 3′- and 5′-Strand Cleavage Reactions Catalyzed by the Fpg Protein from *Escherichia coli* Occur Via Successive *β*- and *δ*-Elimination Mechanisms, Respectively, *Biochemistry 35*, 659−665.
16. Cuniasse, Ph., Sowers, L. C., Eritja, R., Kaplan, B., Goodman, N. F., Cognet, J. A. H., LeBret, M., Guschlbauer, W., and Fazakerly, G. V. (1987) An Abasic Site in DNA. Solution Conformation Determined by Proton NMR and Molecular Mechanics Calculations, *Nucleic Acids Res. 15*, 8003−8022.
17. Cuniasse, Ph., Fazakerly, G. V., Guschlbauer, W., Kaplan, B., and Sowers, L. C. (1990) The abasic site as a challenge to DNA polymerase. A nuclear magnetic resonance study of G, C and T opposite a model abasic site, *J. Mol. Biol. 213*, 303−314.
18. Kalnick, M. W., Chang, C. N., Grollman, A. P., and Patel, D. J. (1988) NMR Studies of Abasic Sites in DNA Duplexes: Deoxyadenosine Stacks into the Helix Opposite the Cyclic Analogue of 2-Deoxyribose, *Biochemistry 27*, 924−931.
19. Kalnick, M. W., Chang, C. N., Johnson, F., Grollman, A. P., and Patel, D. J. (1989) NMR Studies of Abasic Sites in DNA Duplexes: Deoxyadenosine Stacks into the Helix Opposite Acyclic Lesions, *Biochemistry 28*, 3373−3383.
20. Withka, J. M., Wilde, J. A., Bolton, P. H., Mazumder, A., and Gerlt, J. A. (1991) Characterization of Conformational Features of DNA Heteroduplexes Containing Aldehydic Abasic Sites, *Biochemistry 30*, 9931−9940.
21. Goljer, I., Kumar, S., and Bolton, P. H. (1995) Refined Solution Structure of a DNA Heteroduplex Containing an Aldehydic Abasic Site, *J. Biol. Chem. 270*, 22980−22987.
22. Singh, M. P., Hill, G. C., Péoćh, D., Rayner, B., Imbach, J.-L., and Lown, W. (1994) High-field NMR and Restrained Molecular Modeling Studies on a DNA Heteroduplex Containing a Modified Apurinic Abasic Site in the Form of Covalently Linked 9-Aminoellipticine, *Biochemistry 33*, 10271−10285.
23. Coppel, Y., Berthet, N., Coulombeau, C., Coulombeau, C., Garcia, J., and Lhomme, J. (1997) Solution Conformation of an Abasic DNA Undecamer Duplex d(CGCACXCACGC)·d(GCGTGTGTGCG): The Unpaired Thymine Stacks Inside the Helix, *Biochemistry 36*, 4817−4830.
24. Jourdan, M., Garcia, J., Defrancq, E., Kotera, M., and Lhomme, J. (1999) 2′-Deoxyribonolactone Lesion in DNA: Refined Solution Structure Determined by Nuclear Magnetic Resonance and Molecular Modeling, *Biochemistry 38*, 3985−3995.
25. Beger, R. D., and Bolton, P. H. (1998) Structures of Apurinic and Apyrimidinic Sites in Duplex DNAs, *J. Biol. Chem. 273*, 15565−15573.
26. Cline, S. D., Jones, W. R., Stone, M. P., and Osheroff, N. (1999) DNA Abasic Lesions in a Different Light: Solution Structure of an Endogenous Topoisomerase II Poison, *Biochemistry 38*, 15500−15507.
27. Wang, K. Y., Parker, S. A., Goljer, I., and Bolton, P. H. (1997) Solution Structure of a Duplex DNA with and Abasic Site in a dA Tract, *Biochemistry 36*, 11629−11639.
28. Hoehn, S., Turner, C. J., and Stubbe, J. (2001) Solution Structure of an Oligonucleotide Containing an Abasic Site: Evidence for an Unusual Deoxyribose Conformation, *Nucleic Acids Res. 29*, 3413−3423.
29. Ezzitouni, A., Russ, P., and Marquez, V. E. (1997) (1S,2R)-[(Benzyloxy)methyl]cyclopent-3-enol. A Versatile Synthon for the Preparation of 4′,1′a-methano- and 1′,1′a-methanocarbocyclic Nucleosides, *J. Org. Chem. 62*, 4870−4873.
30. Marquez, V. E., Russ, P., Alonso, R., Siddiqui, M. A., Hernandez, S., George, C., Nicklaus, M. C., Dai, F., and Ford, H. (1999) Synthesis of Conformationally Restricted Carbocyclic Nucleosides: The Role of the O(4) Atom in the Key Hydration Step of Adenosine Deaminase, *Helv. Chim. Acta 82*, 2119−2129.
31. States, D. J., Habekorn, R. A., and Ruben, D. J. (1982) A Two-Dimensional Nuclear Overhauser Experiment with Pure Absorption Phase in Four Quadrants, *J. Magn. Reson. 48*, 286−292.
32. Plateau, P., and Gueron, M. (1982) Exchangeable Proton NMR without Base-Line Distortion, Using New Strong-Pulse Sequences, *J. Am. Chem. Soc. 104*, 7310−7311.
33. Sklenar, V., Mishayiro, H., Zon, G., Miles, H. T., and Bax, A. (1986) Assignment of the ^{31}P and ^{1}H Resonances in Oligonucleotides by Two-Dimensional NMR Spectroscopy, *FEBS Lett. 208*, 94−98.
34. Brünger, A. (1993) *XPLOR Version 3.1: A system for X-ray Crystallography and NMR*, Yale University Press, New Haven, CT.
35. Yip, P., and Case, D. A. (1989) A New Method for Refinement of Macromolecular Structures Based on Nuclear Overhauser Effect Spectra, *J. Magn. Reson. 83*, 643−648.
36. Brooks, B. R., Buccoleri, R. E., Olafson, B. D., States, D. J., Swaminathan, S., and Karplus, M. (1983) CHARMM: A program for macromolecular energy, minimization, and dynamics calculations, *J. Comput. Chem. 4*, 187−217.
37. Friedman, R. A., and Honig, B. (1992) The electrostatic contribution to DNA base-stacking interactions, *Biopolymers 32*, 145−159.
38. Majumdar, A., and Hosur, R. V. (1992) Simulation of 2D NMR spectra for determination of solution conformations of nucleic acids, *Prog. NMR Spectrosc. 24*, 109−158.

39. Rinkel, L. J., and Altona, C. (1987) Conformational analysis of the deoxyribofuranose ring in DNA by means of sums of proton−proton coupling constants: a graphical method, *J. Biomol. Struct. Dyn. 4*, 621−649.
40. Lavery, R., and Sklenar, H. (1988) The definition of generalized helicoidal parameters and of axis curvature for irregular nucleic acids, *J. Biomol. Struct. Dyn. 6*, 655−667.
41. de los Santos, C. (1999) Probing DNA Structure by NMR Spectroscopy, in *Comprehensive Natural Products Chemistry* (Kool, E., Ed.) Vol. 7, pp 55−80, Elsevier Science Ltd., Oxford, U.K.
42. Van de Ven, F. J. M., and Hilbers, C. W. (1988) Nucleic acids and nuclear magnetic resonance, *J. Biochem. 178*, 1−38.
43. Mol, C. D., Izumi, T., Mitra, S., and Tainer, J. A. (2000) DNA-bound structures and mutants reveal abasic DNA binding by APE1 DNA repair and coordination, *Nature 403*, 451−456.
44. Wilson, D. M., III, Takeshita, M., Grollman, A. P., and Demple, B. (1995) Incision activity of human apurinic endonuclease (Ape) at abasic site analogues in DNA, *J. Biol. Chem. 270*, 16002−16007.

BI048400C